Supplement for

Method to calculate the aerosol asymmetry factor based on measurements from the humidified nephelometer system

Gang Zhao[1], Chunsheng Zhao[1], Ye Kuang[2], Yuxuan Bian[3], Jiangchuan Tao[2], Chuanyang Shen[1], Yingli Yu[1]

[1]Department of Atmospheric and Oceanic Sciences, School of Physics, Peking University, Beijing, China

[2]Institute for Environmental and Climate Research, Jinan University, Guangzhou 511443, China

[3]State Key Laboratory of Severe Weather, Chinese Academy of Meteorological Sciences, Beijing, 100081, China

1 Measurements sites

The locations where the field campaigns are conducted are shown in Fig. S1. The two campaigns sites are AERONET BEIJING_PKU (PKU) and Gucheng. Filled colors represent the average aerosol optical depth at 550nm during the year of 2016 from Moderate Resolution Imaging Spectroradiometer onboard satellite Aqua.

The PKU station (39°59’ N, 116°18’ E) is located at the northwest of Beijing, between the 4th and 5th ring road. It is 11km from the center of the Megacity Beijing, which is adjacent to Hebei Province and the megacity Tianjin. In the above three cities, the industrial manufacturing has led to heavy air pollution. Gucheng (39°09’ N, 115°44’ E) is located between two megacities (120 km from Beijing and 190 km from Shijiazhuang) of NCP and the pollution conditions of Gucheng can be a good representation of the continental background in the NCP. Details for the Gucheng station can be found at Kuang et al. (2017). The UCAS station (40°24’ N, 116°40’ E) is 60 km away from the center of Beijing and is at the edge of the NCP, which makes it suitable for measuring the regional pollution properties of the NCP (Ma et al., 2016).

The UCAS and PKU locate on the edge of the North China Plain. When the wind direction is south or southeast, the pollutions from the megacity Tianjin and Hebei Province are brought and can significantly influence the pollution condition. However, when the west or northwest wind prevails, the wind brings the relative clean air and the surrounding is less polluted.

2 Determine the n_{tree} and n_{pre} for the random forest machine learning model

For different number of trees (n_{tree}) and n_{pre}, the accuracy of the random forest machine learning model and the time for running the model would change. For different numbers of n_{pre}, the accuracy and the time for running the model would change too.

The influence of the n_{tree} on the accuracy of the model and the times for training the model is studied to

determine the best n_{tree} for the model. The input data of the model come from the dataset of Gucheng and the test data comes from the dataset of PKU. Different values of n_{tree} are used in the model and then the time for running the model the accuracy of the model is compared. The accuracy of the model is estimated by comparing the calculated g values (g_{Mie}) and the predicted g values by the random forest machine learning model (g_{ML}) of PKU. The correlation coefficient (R^2) between g_{Mie} and g_{ML}, the mean relative differences between g_{Mie} and g_{ML}, and the standard deviation (Std) of the relative differences between g_{Mie} and g_{ML} are studied. The results of different n_{tree} are shown in fig. S2. From fig. S2, we can see that the R^2 increases with the increment of n_{tree} from 0.934 to 0.95 when n_{tree} is lower than 32 and changes slightly when n_{tree} is larger than 32, which means that the random forest machine learning model can increase the accuracy of predicting g with the increment of n_{tree} when n_{tree} is lower than 32. At the same, the mean relative difference between g_{Mie} and g_{ML} is all the time lower than 1%, which means that the estimated g is unbiased from the random forest machine learning model. The Std fluctuates between 1% and 1.2% which is also a very small value. The time of training the model increases with the increment of n_{tree} form 0.2s to 1.2s when the n_{tree} increase from 2 to 100. However, the time for predicting the data is slightly changed with the increment of n_{tree}. Therefore, the time of running the model is not a main concerning when choosing the n_{tree}. With the discussion above, the n_{tree} is chosen to be 32 with the accuracy and time of running the model taken into consideration.

Different input parameters can result in different behavior of the machine learning model. The number of n_{pre} is also changed to test the performance of the model by changing the input parameters. From section 3.1.2 of the manuscript, it is obviously that the κ and RH is necessary when predicting the g. We discussed the accuracy of the model by using different combinations of the scattering coefficient and back-scattering coefficient as the input of the random forest machine learning model. There are total six group of tests were carried out. These tests contains (1) all of the three σ_{sca} and three β_{sca}; (2) two σ_{sca} and two β_{sca}; (3) one σ_{sca} and one β_{sca}; (4) three σ_{sca}; (5) three β_{sca} and (6) single parameters of the σ_{sca} or β_{sca}. The details of the tests and the results are shown in Table. S1. These results include the R^2, the mean relative differences and the Std of the relative differences between g_{Mie} and g_{ML}.

From table. S1, the model can work well in test (1) as the R^2 can reach 0.949 and the relative difference is 0.8 ± 1.28. For those of tests (2), the best results come from the test that using the σ_{sca} and β_{sca} at 525 and 635nm with R^2=0.962 and mean value of 1.3 ± 1.32. Despite the fact that the R^2 is slightly higher than that of test (1), both the mean and the standard deviation of the relative difference between g_{Mie} and g_{ML} is larger than that of (1). However, the test that uses the σ_{sca} and β_{sca} at 525nm only at test (3) gets almost the same result. The results of the other tests are much worse than test (1). From test (4) and (5), the corresponding R^2 is much lower when the σ_{sca} and β_{sca} are not used as the input at the same time. It is

concluded that the backscattering coefficient is very important for estimating the g.

For these tests of test (1), the third one in test (2) and the second one in test (3), it is hard to decide which group to be best one as the input parameters. However, it is concluded the test (1) is the most stable one when comparing the mean $\pm$ std of the relative difference. At the same time, the time for predicting the g values using test (1), (2) and (3) does not have clear differences. Thus, the three σ_{sca}, three β_{sca}, κ and RH are chosen as the input of the model and the n_{pre} is set to be eight.

3 The optical closure studies

To avoid the inaccuracy from the instrument, we compared the measured σ_{sca} from the nephelometer and calculated σ_{sca} from Mie scattering theory. The data, where the relative difference between measured σ_{sca} and calculated σ_{sca} are within 30%, are used to for analysis in the study. Fig. S3 gives the comparison results of the σ_{sca} at Gucheng. The measured σ_{sca} and calculated σ_{sca} show good consistence.

4 Parameterization of aerosol vertical distributions

Liu et al. (2009) studied vertical profiles of aerosol total number concentration (Na) with aircraft measurements, and derived a parameterized vertical distribution. In this scheme, Na is constant in the mixed layer, with a transition layer where it linearly decreases and an exponential decrease of Na above the transition layer. The same parameterized scheme proposed by Liu et al. (2009) is adopted by this study as shown in fig. S4(b). Both the study of Liu et al. (2009) and Ferrero et al. (2010) manifest that the dry aerosol PNSD in the mixed layer varies little. The shape of the dry aerosol PNSD is assumed constant with height, which means that aerosol PNSD at different heights divided by Na give the same normalized PNSD. The shape of the dry aerosol PNSD is the mean results of the measured aerosol PNSD at Gucheng and PKU. The profile of the aerosol number concentrations is shown in fig. S4(b).

As for the BC vertical distribution, Ferrero et al. (2011) and Ran et al. (2016) demonstrate that BC mass concentration in the mixed layer remains relatively constant and decreases sharply above the mixed layer. According to this, the parameterization scheme of BC vertical distribution is assumed to be the same as that of aerosol. The BC mass concentration at the surface is the mean results of the measured BC mass concentration at Gucheng and PKU. The shape of the size-resolved BC mass concentration distribution is also assumed to be the same in the vertical direction and the BC size-resolved distribution used by Ma et al. (2012) is used in this study.

With the above assumptions, the aerosol optical properties at each height can be calculated. Fig. S5 shows one of the calculated aerosol optical profiles of the aerosol extinction coefficient, aerosol single scattering albedo and aerosol asymmetry factor.

The corresponding profiles of RH and temperature are shown in fig. S4(a).

5 Aerosol particle properties at different sites

Fig. S6 gives the measured distribution of the aerosol particle number size distrubion (PNSD) at Gucheng, PKU and UCAS. The read line gives mean results of aerosol PNSD and the read line gives the median aeorosl PNSD. At the same time, the aerosol PNSD at the ambient relative humidity are calculated by using the measured aerosol PNSD, the ambient RH and the aerosol hygroscopic growth factor κ, which is derived from the datasets of the humidified nephlometer (Kuang et al., 2017). At the same time, we calculated the aerosol scattering coefficient distibution under the dry condition by using the Mie scattering theory and the measured aerosol PNSD. There are totoal 8613 and 5298 different aerosol PNSD are measured at Gucheng and PKU respectively.

From fig. S6, there are large partitions of small particles that are lower than 60nm at PKU and UCAS. However, these particles, which are lower than 100nm, contribute little to the total aerosol scattering. The aerosol PNSD at PKU is more dispersed than that of the Gucheng and UCAS, which corresponds to a larger variation in the g values. From fig. S6 (h), (i) and (j), the size distribution of the aerosol scatter coefficient at around 500nm contributes less to the scatter coefficient at PKU than at that of the Gucheng and PKU. Thus these particles with the diameter larger than 500nm contribute more to the aerosol scattering coefficient. As g_{Mie} increase with the aerosol diameter, the aerosol g_{Mie} under dry conditions at PKU tends to be larger than that at Gucheng and UCAS.

However, ambient g_{Mie} values have different patterns at different sites, as shown in Fig. 1 (h), (i) and (j). The variations of ambient g_{Mie} values are mainly resulted from the variation of the aerosol hygroscopic growth under the ambient condition, which is highly related to the ambient RH. The g_{Mie} value is significantly influenced by RH when the RH is higher than 80%, which will be detailed in section 4.1.2. Ambient g_{Mie} values at Gucheng, PKU and UCAS can vary from 0.57 to 0.8, 0.55 to 0.76 and 0.56 to 0.72 respectively, comparable to those of Andrews et al. (2006), which range from 0.59 to 0.72.

6 Influence of aerosol complex refractive index on g values.

In our study, the complex refractive index of the light absorging carbonaceous aerosol (LAC) is 1.80+0.54i, and the corresponding values of the aerosol less absorbing aerosol components (inclued inorganic salts, acids, and most of the organic compounds) is $1.53+10^{-7}$i. The value of the refractive index for LAC is in accordance with that used in (Ma et al., 2012;Kuang et al., 2016).

In the folloing parts, the n_{non} and i_{non} refer to the real and imaginary part of the refractive index of less absorbing components and the n_{BC} and i_{BC} refer to the real and imaginary part of the refracitve index of LAC.

For LAC, no accurate refractive index is valid in open literatures, and a variety of values for its refractive index have been used in different climate and aerosol optical models (Bond et al., 2013). Table S2 lists some of the values of the refrative index for the LAC.

For less absorbing components, the refractive indices of different less absorbing aerosol species in the open literature are listed in table S3. The imaginary part of the refractive indices are very small and close to zero. In this study, the i_{non} is assumed to be 10^{-7}. The real part of the refractive indices also don't vay much and the range is small. The filter-based chemical composition results of Liu et al. (2014) demonstrate that sulfate, nitrate and organic matter dominate the composition of the continential aeorsol particles of the accumulation mode. This means that although the chemical composition of less absorbing components varies, the n_{non} will locate within a small range. The n_{non} is assumed to be 1.55 in this research. With this values of refracitve index of less absorbing components, good agreement is achived between calculated and measured scattering coefficients (see section 3 of this suplementary matirial). It is noteworthy that the magnitude of the imaginary parts fo the refractive indices of different less absorbing compoents shown in table S3 range from 0 to 10^{-3}. To insure the rationality of the usage of i_{non}, we cacluate the different g values under different i_{non} conditions at 532nm by using the mean value of the masured aerosol PNSD, aerosol BC mass concentration, aerosol hygroscopicity and the mean mixing state during the observation period of Gucheng. Fig. S7 gives the calculated g values at different RH and the absolute difference between the results of different i_{non}. It can be seen from this figure that even the i_{non} changes significantly, it has negligible impacts on the calculated g. The absolute difference of the g values decrase with the increment of RH because the relative differences of i_{non} of the less absorbing components are smaller at high RH.

Moreover, a Monte Carlo simulation was applied to investigate the influence of the uncertainties of refractive indices of core and shell on calculation of g at different RH by using the Mie theory. The uncertainties of the input parameters for the simulation are listed in Table S4 and those uncertainties are in accordance with that of Cheng et al. (2008) and Ma et al. (2012). The other input of the Mie theory is the mean value of the measured PNSD, aerosol BC mass concentration, aerosol hygroscopicity and the mean mixing state during the observation of Gucheng. The uncertainties of g at the RH range of 30% and 90% with a step of 1% are simulated. For each RH, the simulation were carried out for 20000 times. The simulated results are shown in fig. S8. The results demonstrate that the uncertainties for g are small and less than 0.004. However, the variation of g resulted from aerosol population are 0.1.

By all accounts, the aerosol refractive indices of less absorbing components and LAC has little influence on the aerosol g.

6 Comparison of the parameterized g values

Fig. S9 shows the comparison of the calculated g values from the Mie scattering model and the parameterized g values from the Wiscombe and Grams (1976), with the parameterisation scheme of

$$g = -7.143889 \cdot b^3 + 7.464439 \cdot b^2 - 3.96356 \cdot b + 0.9893 \qquad (1)$$

where b is the hemispheric backscatter fraction. From fig.S9, the parameterized g values are prevalently larger than the calculated ones for about 10%. When measured σ_{sca} is smaller, the deviations get larger. This finding shows that the previously established parameterization scheme is not applicable in the NCP.

Andrews, E., Sheridan, P. J., Fiebig, M., McComiskey, A., Ogren, J. A., Arnott, P., Covert, D., Elleman, R., Gasparini, R., Collins, D., Jonsson, H., Schmid, B., and Wang, J.: Comparison of methods for deriving aerosol asymmetry parameter, Journal of Geophysical Research, 111, 10.1029/2004jd005734, 2006.

Bond, T. C., and Bergstrom, R. W.: Light Absorption by Carbonaceous Particles: An Investigative Review, Aerosol Sci. Technol., 40, 27-67, 10.1080/02786820500421521, 2006.

Bond, T. C., Doherty, S. J., Fahey, D. W., Forster, P. M., Berntsen, T., DeAngelo, B. J., Flanner, M. G., Ghan, S., Karcher, B., Koch, D., Kinne, S., Kondo, Y., Quinn, P. K., Sarofim, M. C., Schultz, M. G., Schulz, M., Venkataraman, C., Zhang, H., Zhang, S., Bellouin, N., Guttikunda, S. K., Hopke, P. K., Jacobson, M. Z., Kaiser, J. W., Klimont, Z., Lohmann, U., Schwarz, J. P., Shindell, D., Storelvmo, T., Warren, S. G., and Zender, C. S.: Bounding the role of black carbon in the climate system: A scientific assessment, J Geophys Res-Atmos, 118, 5380-5552, 10.1002/jgrd.50171, 2013.

Cheng, Y. F., Wiedensohler, A., Eichler, H., Su, H., Gnauk, T., Brüggemann, E., Herrmann, H., Heintzenberg, J., Slanina, J., Tuch, T., Hu, M., and Zhang, Y. H.: Aerosol optical properties and related chemical apportionment at Xinken in Pearl River Delta of China, Atmospheric Environment, 42, 6351-6372, https://doi.org/10.1016/j.atmosenv.2008.02.034, 2008.

Covert, D. S., Heintzenberg, J., and Hansson, H.-C.: Electro-optical Detection of External Mixtures in Aerosols, Aerosol Sci. Technol., 12, 446-456, 10.1080/02786829008959359, 1990.

D'Almeida, G. A., Koepke, P., and Shettle, E. P.: Atmospheric Aerosols: Global Climatology and Radiative Characteristics, Journal of Medical Microbiology, 54, 55-61, 1991.

Dalzell, W. H., and Sarofim, A. F.: Optical Constants of Soot and Their Application to Heat-Flux Calculations, Journal of Heat Transfer, 91, 100-104, 10.1115/1.3580063, 1969.

Ferrero, L., Perrone, M. G., Petraccone, S., Sangiorgi, G., Ferrini, B. S., Lo Porto, C., Lazzati, Z., Cocchi, D., Bruno, F., Greco, F., Riccio, A., and Bolzacchini, E.: Vertically-resolved particle size distribution within and above the mixing layer over the Milan metropolitan area, Atmospheric Chemistry and Physics, 10, 3915-3932, 2010.

Ferrero, L., Mocnik, G., Ferrini, B. S., Perrone, M. G., Sangiorgi, G., and Bolzacchini, E.: Vertical profiles of aerosol absorption coefficient from micro-Aethalometer data and Mie calculation over Milan, Science of the Total Environment, 409, 2824-2837, 2011.

Hasan, H., and Dzubay, T. G.: Apportioning light extinction coefficients to chemical species in atmospheric aerosol, Atmospheric Environment (1967), 17, 1573-1581, https://doi.org/10.1016/0004-6981(83)90310-4, 1983.

Hess, M., Koepke, P., and Schult, I.: Optical Properties of Aerosols and Clouds: The Software Package OPAC, Bulletin of the American Meteorological Society, 79, 831-844, 1998.

Kuang, Y., Zhao, C. S., Tao, J. C., Bian, Y. X., and Ma, N.: Impact of aerosol hygroscopic growth on the direct aerosol radiative effect in summer on North China Plain, Atmospheric Environment, 147, 224-233, 2016.

Kuang, Y., Zhao, C., Tao, J., Bian, Y., Ma, N., and Zhao, G.: A novel method for deriving the aerosol hygroscopicity parameter based only on measurements from a humidified nephelometer system, Atmos. Chem. Phys., 17, 6651-6662, 10.5194/acp-17-6651-2017, 2017.

Liu, H. J., Zhao, C. S., Nekat, B., Ma, N., Wiedensohler, A., van Pinxteren, D., Spindler, G., Müller, K., and Herrmann, H.: Aerosol hygroscopicity derived from size-segregated chemical composition and its parameterization in the North China Plain, Atmospheric Chemistry and Physics, 14, 2525-2539, 10.5194/acp-14-2525-2014, 2014.

Liu, P., Zhao, C., Zhang, Q., Deng, Z., Huang, M., Xincheng, M. A., and Tie, X.: Aircraft study of aerosol vertical distributions over Beijing and their optical properties, Tellus Series B-Chemical & Physical Meteorology, 61, 756–767, 2009.

Ma, N., Zhao, C. S., Müller, T., Cheng, Y. F., Liu, P. F., Deng, Z. Z., Xu, W. Y., Ran, L., Nekat, B., van Pinxteren, D., Gnauk, T., Müller, K., Herrmann, H., Yan, P., Zhou, X. J., and Wiedensohler, A.: A new method to determine the mixing state of light absorbing carbonaceous using the measured aerosol optical properties and number size distributions, Atmos. Chem. Phys., 12, 2381-2397, 10.5194/acp-12-2381-2012, 2012.

Ma, N., Zhao, C., Tao, J., Wu, Z., Kecorius, S., Wang, Z., Größ, J., Liu, H., Bian, Y., Kuang, Y., Teich, M., Spindler, G., Müller, K., van Pinxteren, D., Herrmann, H., Hu, M., and Wiedensohler, A.: Variation of CCN activity during new particle formation events in the North China Plain, Atmospheric Chemistry and Physics, 16, 8593-8607, 10.5194/acp-16-8593-2016, 2016.

Morgan, W. T., Allan, J. D., Bower, K. N., Esselborn, M., Harris, B., Henzing, J. S., Highwood, E. J., Kiendler-Scharr, A., McMeeking, G. R., Mensah, A. A., Northway, M. J., Osborne, S., Williams, P. I., Krejci, R., and Coe, H.: Enhancement of the aerosol direct radiative effect by semi-volatile aerosol components: airborne measurements in North-Western Europe, Atmospheric Chemistry and Physics (ACP) & Discussions (ACPD), 2010.

Ouimette, J. R., and Flagan, R. C.: The extinction coefficient of multicomponent aerosols, Atmospheric Environment (1967), 16, 2405-2419, https://doi.org/10.1016/0004-6981(82)90131-7, 1982.

Ran, L., Deng, Z., Xu, X., Yan, P., Lin, W., Wang, Y., Tian, P., Wang, P., Pan, W., and Lu, D.: Vertical profiles of black carbon measured by a micro-aethalometer in summer in the North China Plain, Atmospheric Chemistry and Physics, 16, 10441-10454, 10.5194/acp-16-10441-2016, 2016.

Seinfeld, J. H., Pandis, S. N., and Noone, K.: Atmospheric Chemistry and Physics: From Air Pollution to Climate Change, Environment Science & Policy for Sustainable Development, 40, 26-26, 1998.

Sloane, C. S.: Optical properties of aerosols of mixed composition, Atmospheric Environment (1967), 18, 871-878, https://doi.org/10.1016/0004-6981(84)90273-7, 1984.

Wiscombe, W. J., and Grams, G. W.: The Backscattered Fraction in two-stream Approximations, J Atmos Sci, 33, 2440-2451, 10.1175/1520-0469(1976)033-2440, 1976.

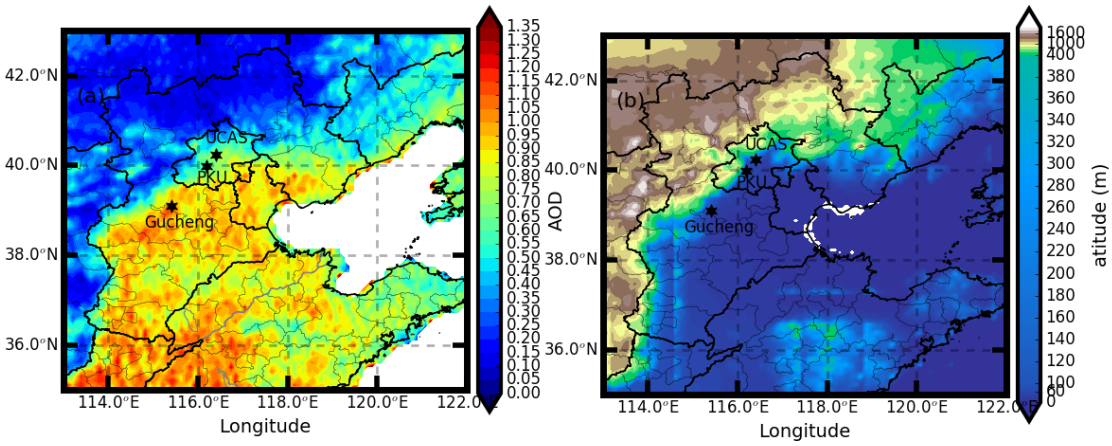

Figure S1: Measurement site of PKU, Gucheng, and UCAS (marked up with stars). Filled colors represent (a) the average aerosol optical depth at 550nm during the year of 2016 from Moderate Resolution Imaging Spectroradiometer onboard satellite Aqua, (b) the topography of the NCP.

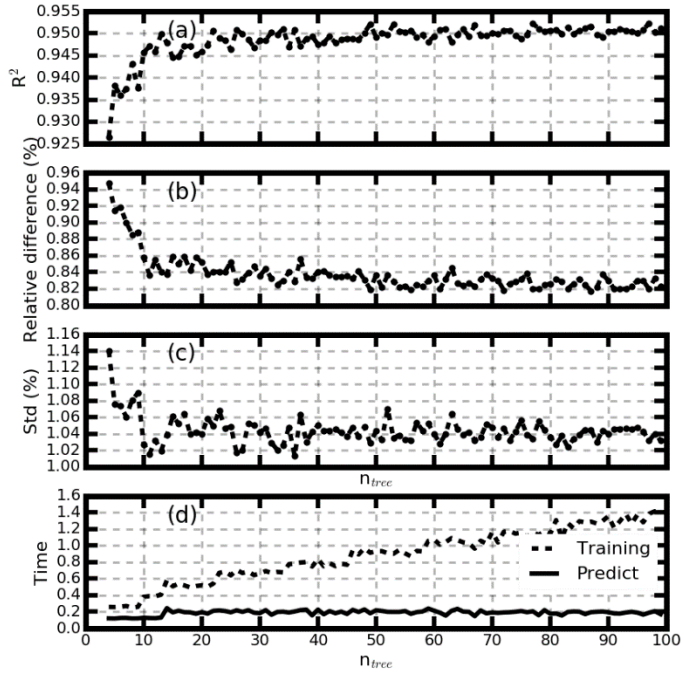

Figure S2. The comparison of g_{ML} and $g_{Mie,dry}$ under different values of n_{tree}. The panels give (a) the correlation coefficient, (b) the mean value of the difference, (c) the standard deviation of the difference valued between g_{ML} and $g_{Mie,dry}$ and (d) the times for running the machine learning model.

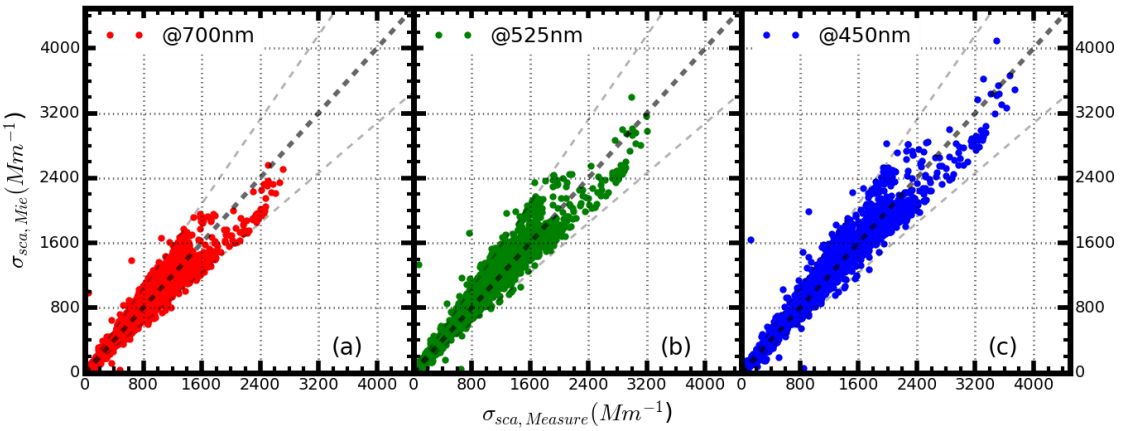

Figure S3. The comparison of the measured σ_{sca} and calculated σ_{sca} at wavelength of **(a)** 700nm, **(b)** 525nm, and **(c)** 450nm. The 1:1 line, and 30% relative difference line are shown in black dotted.

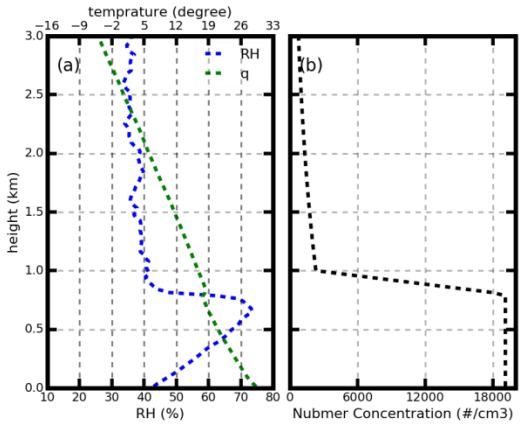

Figure S4. The mean RH, temperature, and aerosol number concentration profiles.

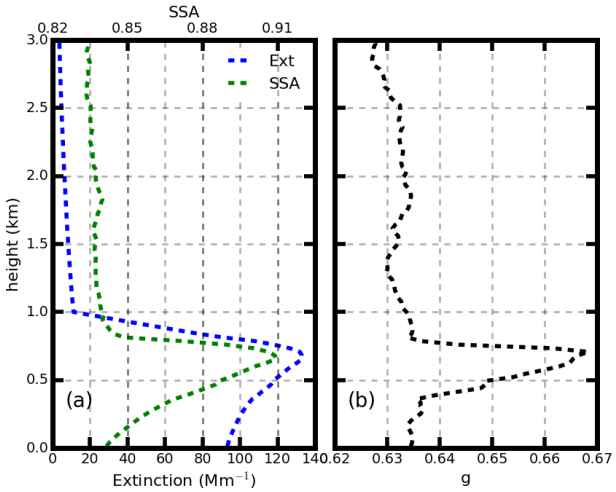

Figure S5. The used profiles of the aerosol extinction coefficient, aerosol single scattering albedo and the aerosol asymmetry factor

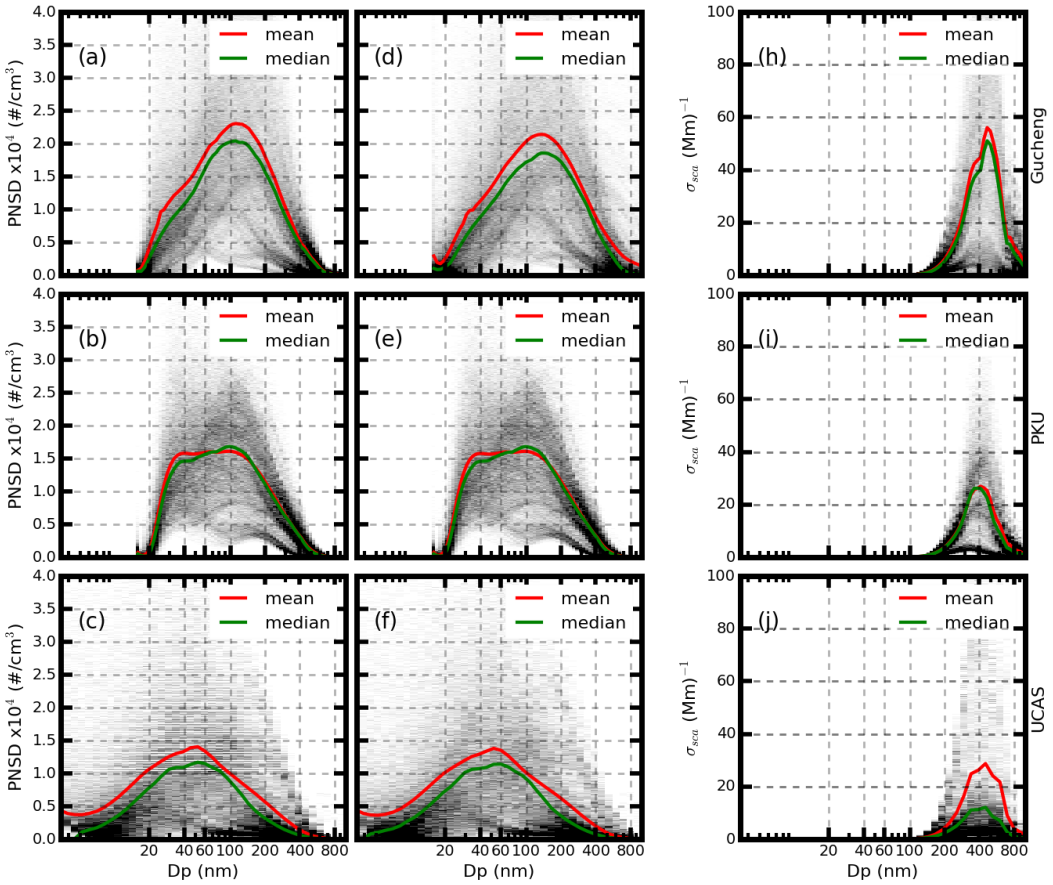

Fig. S6. The distribution of the meaured aerosol PNSD (a) under dry condition and (d) under the ambient condition. Panel (h) shows the size distribution of the scattering coefficient for the measurement site of Gucheng. Fig. (b), (e), i) are the same as fig. (a), (d), (h). but the fig. (b), (e) and (i) is the meausurment result at PKU. Fig. (c), (f), (j) fore the result at UCAS. The read and green lines give the mean and median results of the corresponding datasets respectively.

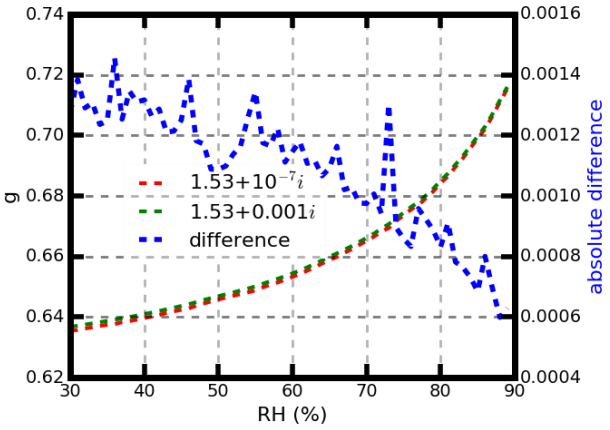

Figure S7. The calculated g under different RH using the complex refractive index of $1.53+10^{-7}$i (read line) and 1.53+0.001i (green line). The blue dotted line shows the absolute difference of the g values under different RH by using the above two refractive index.

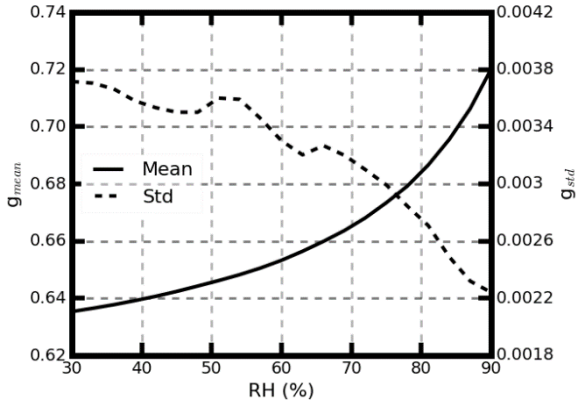

Figure S8. The calculated mean g values and the standard deviation of the g values of the Monte Carlo simulation.

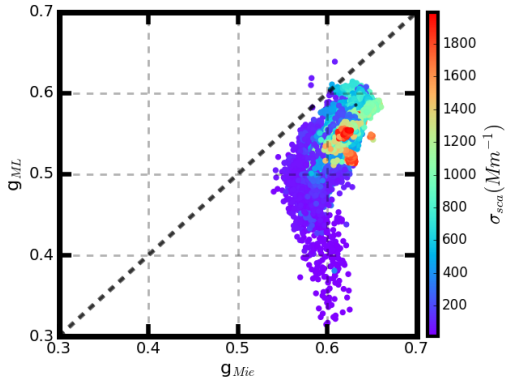

Figure S9. Comparison of the calculated dry g values from the Mie Model and the parameterized g values from Wiscombe and Grams (1976). Colors of these dots represent the measured σ_{sca} corresponding to the time of g value.

Table S1. The influence of the input parameters on the model performance.

N	$\sigma_{sca,635}$	$\sigma_{sca,525}$	$\sigma_{sca,450}$	$\beta_{sca,635}$	$\beta_{sca,525}$	$\beta_{sca,450}$	R^2	Mean±Std (%)[*1]
1	True[*2]	True	True	True	True	True	0.955	0.8±1.28
2	True	True	False	True	True	False	0.936	0.9±1.36
	True	False	True	True	False	True	0.939	0.8±1.36
	False	True	True	False	True	True	0.962	1.3±1.32
3	True	False	False	True	False	False	0.864	0.7±1.79
	False	True	False	False	True	False	0.961	1.7±1.32
	False	False	True	False	False	True	0.936	2.2±1.25
4	True	True	True	False	False	False	0.613	1.4±2.75
	False	False	False	True	True	True	0.817	2.3±1.99
5	True	True	False	False	False	False	0.568	1.4±2.90
	True	False	True	False	False	False	0.588	2.3±2.82
	False	True	True	False	False	False	0.624	2.3±2.75
6	True	False	False	False	False	False	0.401	2.6±3.3
	False	True	False	False	False	False	0.386	2.7±3.39
	False	False	True	False	False	False	0.355	2.8±3.49
	False	False	False	True	False	False	0.323	2.9±3.58
	False	False	False	False	True	False	0.344	2.8±3.52
	False	False	False	False	False	True	0.325	2.9±3.56

[*]1. The mean and the standard deviation of the relative difference between the g_{ML} and g_{mie}.
[*]2. If the value is True, the corresponding parameter is used as the input parameter of the random forest machine learning model.

Table S2. Refractive indices of LAC in open literatures at wavelength of 550nm.

Literature	Refrective index of LAC
(Dalzell and Sarofim, 1969)	1.56+0.56i
(Ouimette and Flagan, 1982)	1.56+0.47i
(Hasan and Dzubay, 1983)	1.97+0.65i
(Sloane, 1984)	1.90+0.55i
(Covert et al., 1990)	1.95+0.66i
(Hess et al., 1998)	1.74+0.44i
(Seinfeld et al., 1998)	1.96+0.66i
(Bond and Bergstrom, 2006)	1.95+0.79i

Table S3. The refractive indices of different less absorbing species.

Literature	S1*	S2*	S3*	S4*	S5*	S6*	S7*
(D'Almeida et al., 1991)	$1.43+10^{-8}i$						
(Morgan et al., 2010)	1.53+0i	1.60+0i				1.63+0.021i	
(Sloane, 1984)	1.53+0i					1.55+0i	1.53+0.005i
(Cheng et al., 2008)			$1.54+10^{-7}i$	$1.54+10^{-7}i$	$1.54+10^{-7}i$	1.55+0.001i	1.58+0.005i

*S1: Ammonium Sulfate

S2: Ammonium Nitrate

S3: Nitrate

S4: Non-Sea-Salt Sulfate

S5: Sea Salt

S6: Organic Matter

S7: Residue

Table S4. Uncertainties of the input parameters for Monte Carlo simulation, giving in terms of one standard deviation. Uncertainties of the input parameters for Monte Carlo simulation, giving in terms one standard deviation (σ,%)

Parameter	Standard deviation (σ,%)
n_{non}=1.55	0.5
i_{non}=10^{-7}	0
n_{BC}=1.80	5
i_{BC}=0.54	6.6